Quantum Interference Channeling at Graphene Edges

Heejun Yang, Andrew J Mayne, Mohamed Boucherit, Geneviève Comtet, Gérald Dujardin, Young Kuk

Quantum interference channeling at graphene edges

Heejun Yang,[1,2] Andrew J. Mayne,[1] Mohamed Boucherit,[1] Geneviève Comtet,[1] Gérald Dujardin,[1] Young Kuk[2]

[1]Laboratoire de Photophysique Moléculaire, CNRS, Bât. 210, Univ Paris Sud, 91405 Orsay, France

[2]Department of Physics and Astronomy, Seoul National University, 151-747 Seoul, Korea

andrew.mayne@u-psud.fr

RECEIVED DATE

Corresponding author: andrew.mayne@u-psud.fr

Abstract

Electron scattering at graphene edges is expected to make a crucial contribution to the electron transport in graphene nanodevices by producing quantum interferences. Atomic-scale scanning tunneling microscopy (STM) topographies of different edge structures of monolayer graphene show that the localization of the electronic density of states along the C-C bonds, a property unique to monolayer graphene, results in quantum interference patterns along the graphene carbon bond network, whose shapes depend only on the edge structure and not on the electron energy.

Graphene nanoribbons have attracted much attention recently for their quasi-one dimensional electronic properties[1] such as the opening of an energy gap,[2,3] with applications in spintronics[4] and as field-effect transistors.[5,6] Resistivity measurements have highlighted the influence of edges in the electron transport properties for narrow graphene nanoribbons (width < 40 nm).[5] However, the exact contributions of edges are still unknown, despite theoretical and experimental studies of edge states.[7,8] These indicate a high electronic density near the Fermi level localized at edges, that could possibly affect the electrical properties of graphene nanoribbons. Electron scattering at graphene edges is also expected to contribute crucially to the electron transport by producing quantum interferences. This has not been investigated so far as it requires a real atomic-scale resolution control of the edge structure.

In this letter, we investigate quantum interferences at edges of monolayer graphene from atomic-scale scanning tunneling microscopy (STM) topographies of different edge structures; irregular armchair, mixed armchair and zigzag, and regular armchair. We observe that quantum interferences form high electronic density of states (DOS) patterns along the C-C bonds, whose shapes depend only on the edge structure and not on the electron energy. This observed channeling of quantum interferences along the carbon bond network in monolayer graphene is explained by electron backscattering at edges and the localization of the electronic DOS along the C-C bonds. This also explains the absence of the $2k_F$ component in the Fourier Transform (FT) analysis and beating effects of the interferences. Previous models,[9,10,11,12,13] introducing inter-valley (other than backscattering) and intra-valley scattering, while adequately describing point defects, fail to explain the observed quantum interferences at edges, because they neglect the localization of the electronic DOS along the C-C bonds.

In Figure 1A, an atomically resolved room-temperature STM image shows the hexagonal lattice of the graphene monolayer. The constant-current STM images were obtained at 300 K in ultrahigh-vacuum (UHV) with an Omicron instrument. The graphene layers were grown epitaxially on a highly n-doped 6H-SiC(0001) sample by thermal desorption of silicon at high temperature.[14,15] A systematic preparation of the stable 3x3 Si-rich phase before graphitization and a low pressure (~$1x10^{-10}$ torr) during graphitization, produced surfaces with a very low defect density. The bond width measured from the

DOS profile across the bonds (Figure 1B) has a full-width half-maximum (FWHM) value of 1.4Å and does not vary with the applied voltage (Figure 1C). The electronic density of states (DOS) is clearly localized along the C-C bonds and appears unique to monolayer graphene compared to other carbon-based systems such as poly-aromatic molecules[16] or diamond surfaces[17] where the electronic DOS are delocalized over the phenyl rings or along carbon dimer rows, respectively. In comparison, the STM topography of bilayer graphene is completely different as only three of the six carbon atoms in each hexagon can be seen[9,12,15], however, it has been shown that *Z*(V) spectroscopy can provide an unambiguous distinction between monolayer and bilayer graphene[15] independent of the quality of the STM images. The origin of the localization of the electron DOS along the C-C bond network of monolayer graphene is still under debate. We emphasize that similar STM images are seen whatever the surface voltage: 4 mV,[9,10] -17 mV,[11] -50mV (Figure 1A) and -1V (Figure 2A). Thus in all the tunnel regimes, either weak elastic tunneling into the π bands (low surface voltage) or the more efficient phonon-assisted inelastic tunneling into mixed σ and π states at higher surface voltage,[18,19] the same localization of the electron DOS is observed. This is not a picture specific to the STM since similar localization along the C-C bonds is observed in the high energy transmission electron microscope (HTEM) images of monolayer graphene.[20]

In the STM topography of Figure 2A, quantum interferences parallel to a monolayer graphene edge are clearly seen. The lower terrace (upper part Figure 2A) is composed of the C-rich buffer-layer.[12] No structure is seen on the C-rich layer simply because at 50mV bias we are in the gap of the C-rich layer. However, the C-rich layer can be imaged more easily at higher bias (>1V). In previous STM studies of graphene on SiC, only graphene carpet edges were observed. Here, real graphene edges were produced by choosing a moderate annealing procedure to form monolayer graphene (lower temperature, longer time). In this regime, monolayer graphene is produced with a number of edges. From the atomic-scale topography, the edge in Figure 2A can be described as an irregular arm-chair edge (Figures 2A and 2D - see supplement for edge structure determination). Close to the Fermi level, electrons have a wave vector approximately equal to k_F, i.e. the distance between the Γ and a K point of the Brillouin zone (Figure

2B).[11,12,21,22,23] The corresponding wavelength $\lambda_F = 2\pi/k_F = 3a/2$, where a = 2.46Å. Thus $k_F = 17.4$ nm^{-1} and $\lambda_F = 3.69$ Å. From the STM topography (Figure 2A), we deduce that the quantum interferences have a periodicity of 3.7 Å, i.e. equal to the wavelength λ_F of the interfering waves. This observation is confirmed by the Fourier Transform (FT, inset 2A) which shows only two out of the six possible k-points of the first Brillouin zone with a wave vector, $k = k_F = 17.4$ nm^{-1}, i.e. a periodicity of λ_F. The outer points correspond to the carbon lattice. The FT shows no wave vector at $k = 2k_F$ (i.e. a periodicity of $\lambda_F/2$). However, in metals λ_F waves would produce quantum interferences with a periodicity of $\lambda_F/2$ and a FT k vector, $k = 2k_F$.[24,25,26] We would expect the same here for a backscattering process, where waves propagating in opposite directions are equivalent to large momentum scattering between opposite K points (green arrows, Figure 2B). In previous experiments,[9-12] the occurrence of k_F and the absence of $2k_F$ quantum interferences was ascribed to inter-valley scattering with a 60° angle between the incident, k^i_F and scattered k^s_F vectors (blue arrows, Figure 2C).[9,10,21] This inter-valley scattering was the only way to explain that scattered λ_F waves could produce λ_F periodicity quantum interferences.

In fact, a careful analysis of the real space quantum interferences (QI) shows that QI patterns are seen only when they coincide with C-C bonds near the edge of monolayer graphene, as observed in Figure 2A. By performing the reverse FT on the two k-points and the lattice only, the QI pattern is clearer (Figure 2C). The maxima of the interferences are separated by 3.7 Å, i.e. λ_F. Comparison of the QI positions with respect to the lattice gives the schematic pattern in Figure 2D. The intense DOS lines coincide with the C-C bonds. The dotted lines represent the expected positions of the missing $\lambda_F/2$ ($2k_F$) interferences, but there are no C-C bonds and so no available electronic DOS at this position. Therefore, the absence of $2k_F$ vectors in the FT is due to the localization of the electronic DOS on the C-C lattice; only k_F can be seen. From this result, it appears that the localization of the electronic DOS along the C-C bonds, which is a property unique to monolayer graphene, is crucial to understand why λ_F waves scattered at a graphene edge produce λ_F QI whereas they would produce $\lambda_F/2$ QI at a metal edge.

The quantum interferences in Figure 2E, showing another example of a monolayer graphene edge, are particularly interesting because only one direction is observed with a periodicity of $\lambda_F = 3.7$ Å and an

angle of 60° to the edge. The STM topographies in Figures 2A and 2E, show irregular edge structures whose atomic-structure is smeared out by the quantum interferences themselves. In this case, the irregular armchair structure (Figure 2A) and the mixed zigzag and armchair structure (Figure 2F), are determined using the procedure explained in the supplement. Indeed, the proposed mixed zigzag and armchair structure (Figure 2F), is the only atomic-scale edge structure able to produce interferences in the direction observed. Obviously, the inter-valley scattering with an angle of 60° between the incident, k^i_F and scattered k^s_F vectors, used so far to explain the λ_F periodicity,[9,10] is inadequate because the scattered k^s_F wave would have to propagate beyond the graphene monolayer edge and therefore, could not interfere with the incident k^i_F wave (Figure 2F). However, our model, associating backscattering at the edge with the localization of the electronic DOS, explains the observed λ_F periodicity. Indeed, in this case, the incident k^b_F and scattered $-k^b_F$ waves have opposite directions (Figure 2F) enabling interference to occur and the absence of the $\lambda_F/2$ periodicity is due to the localization of the DOS along the C-C bonds, as explained before.

A more complex quantum interference pattern at a regular arm-chair edge is shown in Figure 3. From the STM topographies in Figures 3A and 3B, we can again correlate perfectly the quantum interference pattern with the C-C bond positions. In fact, the QI pattern can be decomposed into three directions (red, blue and green) as shown in Figure 3C. Note that the direction normal to the edge (red) has two components due to the regular arm-chair structure. The directions at 60° to the edge (blue and green) are similar to the example in Figure 2E. It is the very regular arm-chair structure that allows QIs to be produced in three directions at the same time, whereas irregular structures (Figures 2A and 2E) allow only one direction in each case. We emphasize that in Figure 3, the three directions correspond to quantum interferences with a periodicity of 3.7 Å, i.e. λ_F. This is confirmed in the FT (inset 3A) which clearly shows all six k-points with a $k = k_F = 17.4$ nm^{-1} generated by the QIs. Again, the $2k_F$ QI corresponding to a periodicity of $\lambda_F/2$ are not seen either in the FT or the STM topography because they do not coincide with any C-C bonds. The component normal to the edge (red) could be explained by inter-valley scattering (k^i_F and k^s_F at 60°) and by neglecting the localization of the DOS along the C-C

bonds. However, the other two components (blue and green) cannot be described by such inter-valley scattering for the simple reason that the propagation of the scattered wave k^s_F would be beyond the monolayer graphene edge, preventing interference with k^i_F. Only backscattering (k^b_F and $-k^b_F$ at 180°) and localization of the DOS can explain the blue and green components with a periodicity of λ_F.

Figure 4A shows the FT of the image in Figure 3A. A zoom of one of the k-points (Figure 4A -inset) indicates that each spot has two components separated by $2\delta k = 2.5$ nm^{-1}; this corresponds to a long-range oscillation with a period, $\pi/\delta k = 2.5$ nm (see supplement). The relatively small sized STM topography (10 nm) in Figure 3A results in a lower k-space resolution ($= 2\pi/10$ nm $= 0.6$ nm^{-1}) than in previous studies,[9-11] so that we observed 2 spots at a k-point instead of 2 arcs. However, our priority was to investigate the clearly visible QI in the real-space STM topographies with the FT analysis providing support. Nevertheless, the resolution of 0.6 nm^{-1} in the FT is good enough to separate the two components. An image size of 10 nm is a good compromise between sufficient real-space atomic resolution and a minimum for the FFT analysis. The inverse FT in Figure 4B highlights more clearly the long-range oscillations (beating), in particular the intensity variations across the terrace. A profile (Figure 4C), shows a beat pattern with a period $L_{beat} = 2.5$ nm, and a decay of the maximum intensity as a function of distance,[27] giving an experimental decay length, $L_{decay} = 5.0$ nm. This measured decay length is considered to be due to the non-zero energy spread of the tunnel electrons (-50 meV) combined with a thermal contribution.[24]

At first sight the observation of long range oscillations or beating effects of the quantum interferences in monolayer graphene is surprising. Indeed, similar long wavelength oscillations have been observed in bilayer graphene[9] and single wall nanotubes,[22] but not in monolayer graphene.[10] These effects in bilayer graphene were ascribed to intra-valley scattering, while the intra-valley scattering interferences were thought to be absent in monolayer graphene due to the opposite pseudospin of the interfering waves.[10,23,28] Here, we demonstrate that the long-range oscillations are due to the difference between the Dirac (E_D) and Fermi Energies (E_F) combined with the localization of the electronic DOS along the C-C bonds. The K-points of the 2D Brillouin zone have a finite diameter ($2\delta k$ – Figure 4D) which is given by

the linear dispersion law around the Dirac points ($\delta k = \delta E/\hbar v_F$, $v_F = 10^6$ ms^{-1}).[9,29] The separation between the Dirac energy (E_D) and the Fermi energy (E_F), for monolayer graphene on 6H-SiC(0001) is given by $E_D = E_F - 0.45$ eV.[11,12,23] It follows that for a surface voltage *Vs* = -0.05 eV, tunnel electrons have a minimum energy of 0.40 eV above E_D. At this energy, $2\delta k = 0.15$ Å^{-1}, and the wavelength can take values between $\lambda_1 = \lambda_F + \delta\lambda$ and $\lambda_2 = \lambda_F - \delta\lambda$, ($\lambda_F = 3.69$ Å and $\delta\lambda = 0.15$ Å) (Figure 4D). We can then deduce that the combination of the DOS localized on the C-C bonds (period = $\lambda_F/3$) with a QI of periodicity $\lambda_1 = \lambda_F + \delta\lambda$ will give rise to long-range oscillations as shown in Figure 4E. Each period of the quantum interference results in a shift of λ_1-λ_F relative to the C-C bond positions. Therefore, the accumulated shift of the QI will be equal to the period $\lambda_F/3$ of the C-C bond positions after $n = \lambda_F/3(\lambda_1-\lambda_F)$ periods of the QI. This dephasing creates nodes at regular intervals (Figure 4E). This implies a beat period, $L_{beat} = n.\lambda_1$. So $L_{beat} = \lambda_F.\lambda_1/3(\lambda_1-\lambda_F) = (\lambda_F)^2/3\delta\lambda$. When $\delta\lambda = \pm 0.15$ Å, $L_{beat} = 3.0$ nm compared to our experimental value of 2.5 nm. We conclude that long-range oscillations exist at monolayer graphene edges and can be explained by the matching between QI and the localized DOS along the C-C bonds, without any need to consider intra-valley scattering.

This localization of the DOS along the C-C bonds, which is crucial to understand the QI at monolayer graphene edges, has been neglected in previous studies of QI at point defects because only k-space analysis was possible through the FT of the STM topographies. In neglecting this localization of the DOS, previous studies were forced to invoke intra-valley and inter-valley scattering (other than backscattering) to explain the unique features of QI in graphene. However, we have shown here that inter-valley scattering (other than backscattering) is inadequate to explain QI at both regular arcmchair and the mixed zig-zag - armchair edges.

In conclusion, a real space analysis of STM topographies shows quantum interferences at three differently structured monolayer graphene edges: irregular arm-chair, mixed zig-zag plus arm-chair, and regular arm-chair. The shapes of the QI patterns, the absence of the $\lambda_F/2$ ($2k_F$) periodicity, and long-range oscillations (beating effect), are explained by only backscattering and the localization of the electronic DOS along the C-C bonds. The localization of the electronic DOS along the C-C bonds in

monolayer graphene tells us much more than just the relationship between the QIs and the STM topography. We emphasize that, in the case of metals, quantum interference patterns, free of lattice constraints, strongly depend on the electron energy. This has been exploited for quantum holographic encoding effects.[30,31] The localization of the electronic DOS along the 1.4Å-wide C-C bond network is a property unique to monolayer graphene. This gives rise to quantum interference patterns whose shapes depend only on the edge structure and not on the electron energy. This quantum interference channeling has important consequences for future nano-electronics with graphene. Indeed, we can anticipate that electron transport in nanoribbons will strongly depend on the atomic-scale electronic DOS circuits created by QI,[29,32,33] even though complete calculations of the electron transport taking into account the QI patterns has yet to be achieved. Also, an atomic-scale control of the edge structures of graphene nanoribbons is still a key problem for the engineering of graphene. However, these results herald the possibility of a real quantum interference channeling circuitry.

Acknowledgements. We thank L. Simon, T. Kontos, P. Mallet, M.-L. Bocquet for helpful discussions. The French advanced thematic research network project RTRA 2008-024T provided finance.

Supporting Information Available. The Supporting Information includes 3 figures, and expanded discussions of peripheral findings.

SYNOPSIS TOC

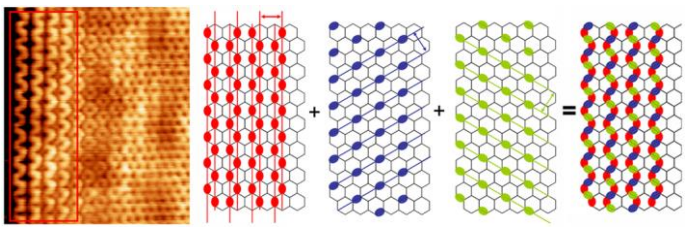

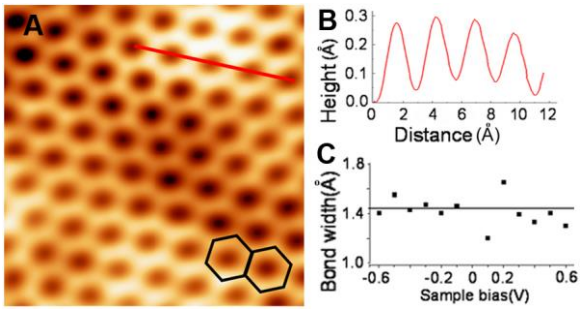

Figure 1: (A) 2 x 2 nm STM topography showing hexagonal structure of monolayer graphene and the localisation of the electronic density of states (DOS) on the carbon lattice (black hexagons). Tunnel conditions: V_S = -0.05 V, I = 1.0 nA. (B) Line profile (red line in a) showing the width of the DOS. (C) The bond width, measured from different STM images, is constant between sample biases of -0.6 and +0.6 V with an average value of 1.4Å.

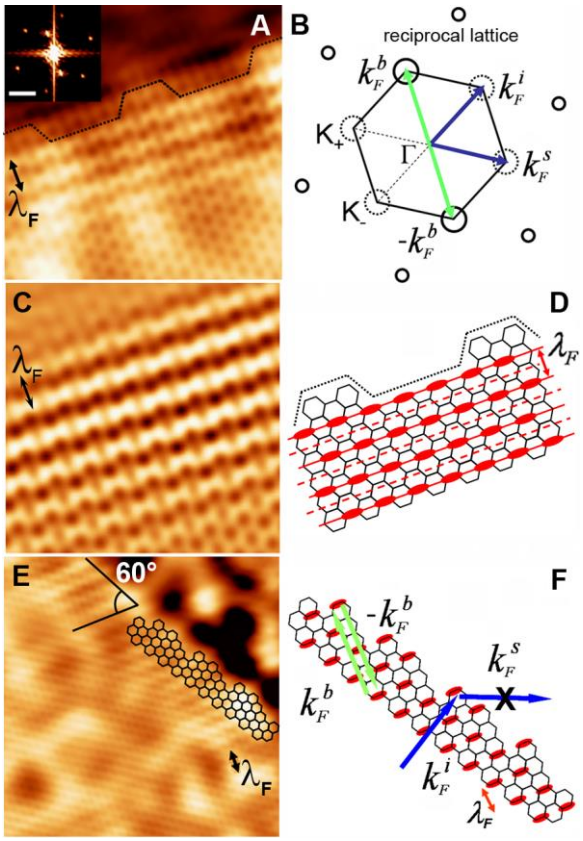

Figure 2: (A) 4.1 x 4.1 nm STM topography showing one-direction quantum interferences (QI) parallel to an irregular graphene monolayer edge (black line, bottom terrace) and corresponding Fourier Transform (inset - Scale bar 20 nm^{-1}) (V_S = -0.05V, I = 0.5 nA). The carbon-rich layer is at the top. (B) Schematic of the 2D Brillouin zone, the K-points generated by the QIs (solid circles), and absent K-points (dotted circles). The k^b_F and $-k^b_F$ vectors (green) indicate normal backscattering and the k^i_F and k^s_F vectors (blue) other inter-valley scattering. The outer small circles indicate the graphene reciprocal lattice points. (C) Inverse FT of the two k-points and lattice vectors shows the detailed QI pattern (3.0 x 3.0 nm). (D) Irregular armchair edge structure (in A) with an envelope (black dotted line). The repeating red oval pattern separated by λ_F represents the intense DOS of the QI (bright features C), coinciding with the carbon lattice. The expected position of $\lambda_F/2$ does not coincide with any C-C bond (red dotted lines). (E) 6.8 x 6.8 nm STM topography of one-direction quantum interferences with a 60° angle to another graphene monolayer edge (edge structure is overlaid). (V_S = -1.0V, I = 0.6nA). (F) Mixed armchair and zig-zag edge structure, indicating allowed backscattering (green) and forbidden inter-valley scattering (blue). The red ovals represent the QI pattern.

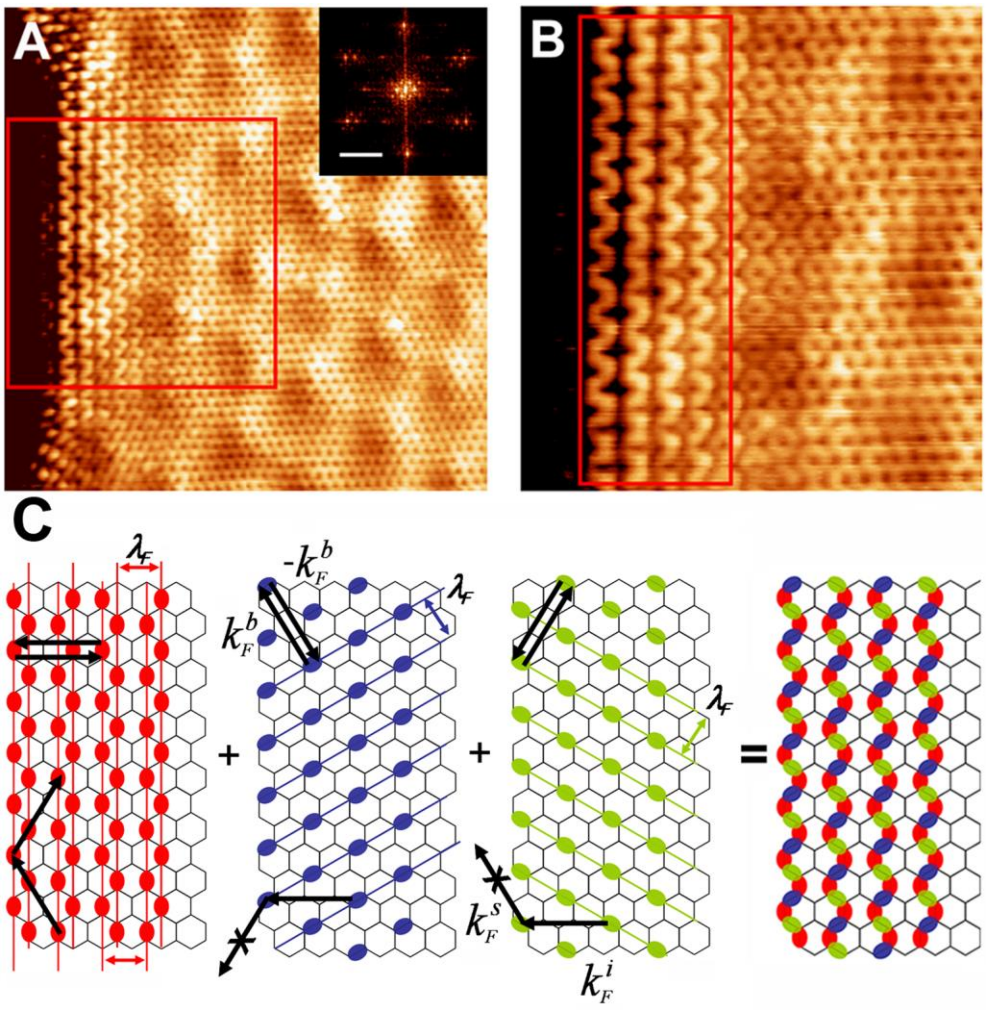

Figure 3: (A) 10 x 10 nm STM topography (V_S = -0.05V, I = 0.5 nA) showing quantum interferences at a regular armchair edge of a graphene monolayer (lower terrace - carbon-rich layer). Inset: Fourier Transform (Scale bar = 20 nm^{-1}). (B) A zoom of the STM image (red square in A) showing the fine detail of the QI. (C) Schematic diagram showing the decomposition of the QIs into three directions; parallel to the edge (red), and at angles of 60° to the edge (blue and green). The periodicity of each component is 3.7 Å (λ_F) and the lines of high intensity DOS coincide with the C-C bonds. In each case, backscattering (k^b_F to $-k^b_F$) and inter-valley scattering (k^i_F to k^s_F) are indicated by the black arrows. Inter-valley scattering is not allowed for the blue and green components as the scattered k^s_F wave would have to propagate beyond the graphene monolayer edge. Combining the three interference directions gives the same pattern observed close to the edge in the STM image (red rectangle in B).

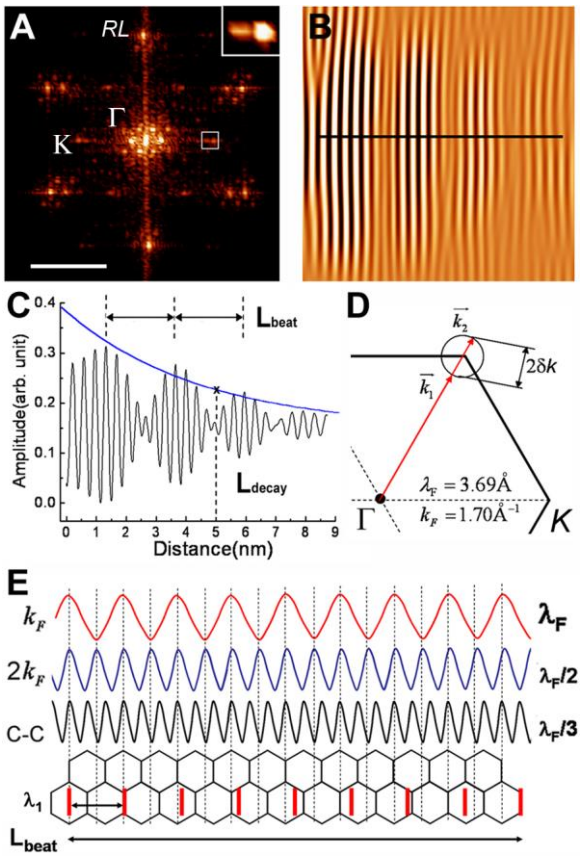

Figure 4: (A) Fourier Transform (FT) of the STM image in Figure 3A (Scale bar = 20 nm^{-1}). The satellite spots around the reciprocal lattice points (RL) correspond to the underlying carbon-rich layer. (inset) Zoom of one k-point (white square in A, size 5.0 x 4.2 nm^{-1}); the two spots, separated by 2δk = 2.5 nm^{-1}, correspond to long-range oscillations. (B) Inverse FT of the pattern near the k-point (A inset). The QI propagates into the terrace with decreasing intensity and clear long-range oscillations. (C) Line profile from B, showing the long-range oscillation (beat pattern), L_{beat} (2.5 nm) and decay length, L_{decay} (5.0 nm). (D) Corner section of the first Brillouin zone from the central Γ–point to one K-point (diameter 2δk). The K-point circle can be reached by two k-vectors, k_1 and k_2. (E) Schematic relationship between the periods of λ_F (k_F), $\lambda_F/2$ ($2k_F$), and the C-C bonds ($\lambda_F/3$) of the hexagonal lattice. For λ_1 = 3.84Å, the interference is in phase with the C-C bonds of the lattice after 8 periods of λ_1 i.e. $8\lambda_F + \lambda_F/3$; giving a beating period, L_{beat} of 3 nm.

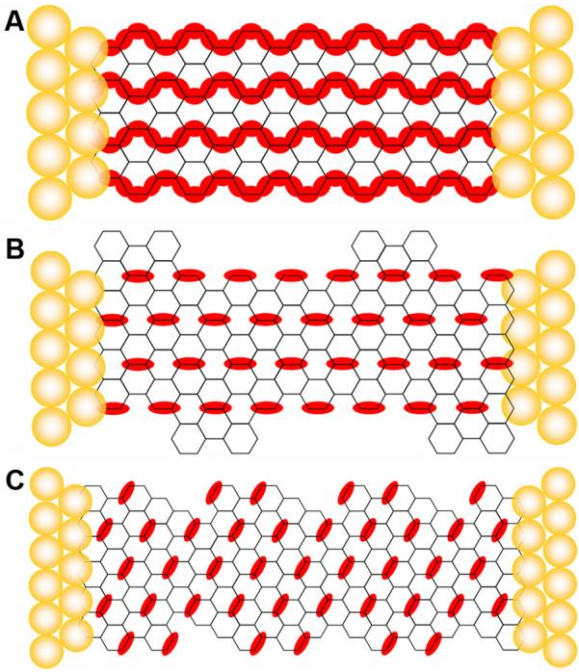

Figure 5: Here, we show schematically the quantum interference channeling that is expected in graphene nanoribbons having the three types of edge structures observed in this study. (A) Regular armchair edges: localization of quantum interferences (red ovals) causes a continuous high density of states (DOS) to be channeled along the C-C network, as in Figure 3, between the metal electrodes (yellow disks). (B) Irregular armchair edge: the DOS is more localized because the quantum interferences form only in the transverse direction (edge corresponding to Figure 2A). (C) Mixed armchair and zig-zag edge: quantum interference is produced only at an angle of 60°with respect to the nanoribbon axis (as in Figure 2E).

[1] Jia, X.; Hofmann, M.; Meunier, V.; Sumpter, B. G.; Campos-Delgado, J.; Romo-Herrera, J. M.; Son, H.; Hseih, Y.-P.; Reina, A.; Kong, J.; Terrones, M.; Dresselhaus, M. S. *Science* **2009**, *323*, 1701-1705.

[2] Son, Y. W.; Cohen, M. L.; Louie, S. G. *Phys. Rev. Lett.* **2006**, *97*, 216803.

[3] Han, M. Y.; Özylimaz, B.; Zhang, Y.; Kim, P. *Phys. Rev. Lett.* **2007**, *98*, 206805.

[4] Son, Y. W.; Cohen, M. L.; Louie, S. G. *Nature* **2006**, *444*, 347-350.

[5] Chen, Z.; Lin, Y.-M.; Rooks, M. J.; Avouris, Ph. *Physica E* **2007**, *40*, 228-232.

[6] Wang, X.; Ouyang, Y.; Li, X. Wang, H.; Guo, J.; Dai, H. *Phys. Rev. Lett.* **2008**, *100*, 206803.

[7] Fujita, M.; Wakabayashi, K.; Nakada, K.; Kusakabe, K. *J. Phys. Soc. Jpn.* **1996**, *65*, 1920.

[8] Kobayashi, Y.; Fukui, K.; Enoki, T.; Kusakabe, K.; Kaburagi, Y. *Phys. Rev. B* **2005**, *71*, 193406.

[9] Rutter, G. M.; Crain, J. N.; Guisinger, N. P.; Li, T.; First, P. N.; Stroscio, J. A. *Science* **2007**, *317*, 219-222.

[10] Brihuega, I.; Mallet, P.; Bena, C.; Bose, S.; Michaelis, C.; Varchon, F.; Magaud, L.; Kern, K.; Veuillen, J.-Y. *Phys. Rev. Lett.* **2008**, *101*, 206802.

[11] Simon, L.; Bena, C.; Vonau, F.; Auble, D.; Nasrallah, H.; Habar, M.; Perruchetti, J. C. *Eur. Phys. J. B* **2009**, *69*, 351-355.

[12] Mallet, P.; Varchon, F.; Naud, C.; Magaud, L.; Berger, C.; Veuillen, J.-Y. *Phys. Rev. B* **2007**, *76*, 041403R.

[13] Bena, C. *Phys. Rev. Lett.* **2008**, *100*, 076601.

[14] Forbeaux, I.; Themlin, J.-M.; Debever, J.-M. *Phys. Rev. B* **1998**, *58*, 16396-16406.

[15] Yang, H.; Baffou, G.; Mayne, A. J.; Comtet, G.; Dujardin, G.; Kuk, Y. *Phys. Rev. B* **2008**, *78*, 041408R.

[16] Repp, J.; Meyer, G.; Paavilainen, S.; Olsson, F. E.; Persson, M. *Science* **2006**, *312*, 1196-1199.

[17] Bobrov, K.; Mayne, A. J.; Dujardin, G. *Nature* **2001**, *413*, 616-619.

[18] Zhang, Y.; Brar, V. W.; Wang, F.; Girit, C.; Yayon, Y.; Panlasigui, M.; Zettl, A.; Crommie, M. F. *Nat. Phys.* **2008**, *4*, 627-630.

[19] Wehling, T. O.; Grigorenko, I.; Lichtenstein, A. I.; Balatsky, A. V. *Phys. Rev. Lett.* **2008**, *101*, 216803.

[20] Girit, Ç. Ö.; Meyer, J. C.; Erni, R.; Rossell, M. D.; Kisielowski, C.; Yang, L.; Park, C.-H.; Crommie, M. F.; Cohen, M. L.; Louie, S. G.; Zettl, A. *Science* **2009**, *323*, 1705-1709.

[21] Ruffieux, P.; Melle-Franco, M.; Gröning, O.; Bielmann, M.; Zerbetto, F.; Gröning, P. *Phys. Rev. B* **2005**, *71*, 153403.

[22] Lemay, S. G.; Janssen, J. W.; van den Hout, M.; Mooij, M.; Bronikowski, M. J.; Willis, P. A.; Smalley, R. E.; Kouwenhoven, L. P.; Dekker, C. *Nature* **2001**, *412*, 617-620.

[23] Bostwick, A.; Ohta, T.; Sellyer, T.; Horn, K.; Rotenberg, E. *Nature Phys.* **2007**, *3*, 36-40.

[24] Hasegawa, Y.; Avouris, Ph. *Phys. Rev. Lett.* **1993**, *71*, 1071-1074.

[25] Sprunger, P. T.; Petersen, L.; Plummer, E. W.; Laegsgaard, E.; Besenbacher, F. *Science* **1997**, *275*, 1764-1767.

[26] Park, J.-Y.; Ham, U. D.; Kahng, S.-J.; Kuk, Y.; Miyake, K.; Hata, K.; Shigekawa, H. *Phys. Rev. B* **2000**, *62*, 16341-16344.

[27] Wahl, P.; Schneider, M. A.; Diekhöner, L.; Vogelgesang, R.; Kern, K. *Phys. Rev. Lett.* **2003**, *91*, 106802.

[28] Katsnelson, M. I.; Novoselov, K. S.; Geim, A. K. *Nature Phys.* **2006**, *2*, 620-625.

[29] Berger, C.; Song, Z.; Li, X.; Wu, X.; Brown, N.; Naud, C.; Mayou, D.; Li, T.; Hass, J.; Marchenkov, A. N.; Conrad, E. H.; First, P. N.; de Heer, W. A. *Science* **2006**, *312*, 1191-1196.

[30] Kliewer, J.; Berndt, R.; Crampin, S. *New J. Phys.* **2001**, *3*, 22.

[31] Moon, C. R.; Mattos, L. S.; Foster, B. K.; Zeltzer, G.; Manoharan, H. C. *Nature Nano.* **2009**, *4*, 167-172.

[32] Tapasztó, L.; Dobrik, G.; Lambin, P.; Biró, L. P. *Nature Nano.* **2008**, *3*, 397-401.

[33] Li, X.; Wang, X.; Zhang, L.; Lee, S.; Dai, H. *Science* **2008**, *319*, 1229-1232.